We are IntechOpen, the world's leading publisher of Open Access books Built by scientists, for scientists

4,800
Open access books available

122,000
International authors and editors

135M
Downloads

Our authors are among the

154
Countries delivered to

TOP 1%
most cited scientists

12.2%
Contributors from top 500 universities

CLARIVATE ANALYTICS BOOK CITATION INDEX INDEXED

WEB OF SCIENCE™

Selection of our books indexed in the Book Citation Index in Web of Science™ Core Collection (BKCI)

Interested in publishing with us?
Contact book.department@intechopen.com

Numbers displayed above are based on latest data collected.
For more information visit www.intechopen.com

11

PV Solar Energy Conversion Using the Behavior Matching Technique

Marcio Mendes Casaro[1] and Denizar Cruz Martins[2]
[1]*Federal University of Technology - Paraná, Ponta Grossa*
[2]*Federal University of Santa Catarina, Power Electronics Institute*
Brazil

1. Introduction

This chapter presents the Behavior Matching technique (Casaro & Martins, 2007; Casaro & Martins, 2008). It is based on DC-DC converters' input I-V characteristics. When a DC-DC converter employs the technique, its duty-cycle and frequency are optimal fixed values. It don't use a control loop for MPPT, but the maximum power point is fastest tracked for rapid solar irradiation changes. A minimal amount of sensors and only one microcontroller are required for PV system operation. There are many options of technique-compatibles DC-DC converters to achieve high frequency isolation and high efficiency. To continue, a brief explanation about how a DC-DC converter can be inserted in a PV system is introduced.

1.1 PV systems

Distributed PV generation systems use switching inverters to extract the maximum power of photovoltaic modules and inject this energy into grid. Grid-current control and MPPT are carried out by inverter in different ways. The following topics explain the state of the art about inverters topologies (Carrasco et al., 2006).

- Single-stage inverter: in one processing stage, MPPT and grid-current control are handled.
- Dual-stage inverter: a DC-DC converter performs the MPPT and a DC-AC one is responsible for the grid-current controlling.
- Multistage inverter: various DC-DC converters are used for the MPPT and only one DC-AC converter takes care of the grid-current control.

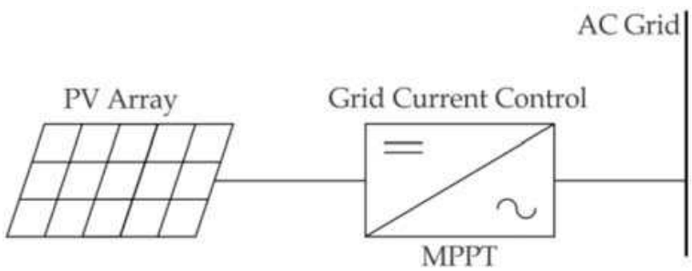

Fig. 1. Inverter without a DC-DC converter.

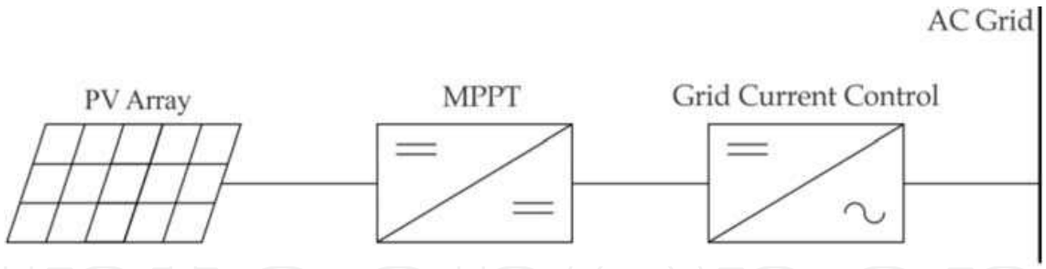

Fig. 2. Photovoltaic energy flowing through two conditioning converters.

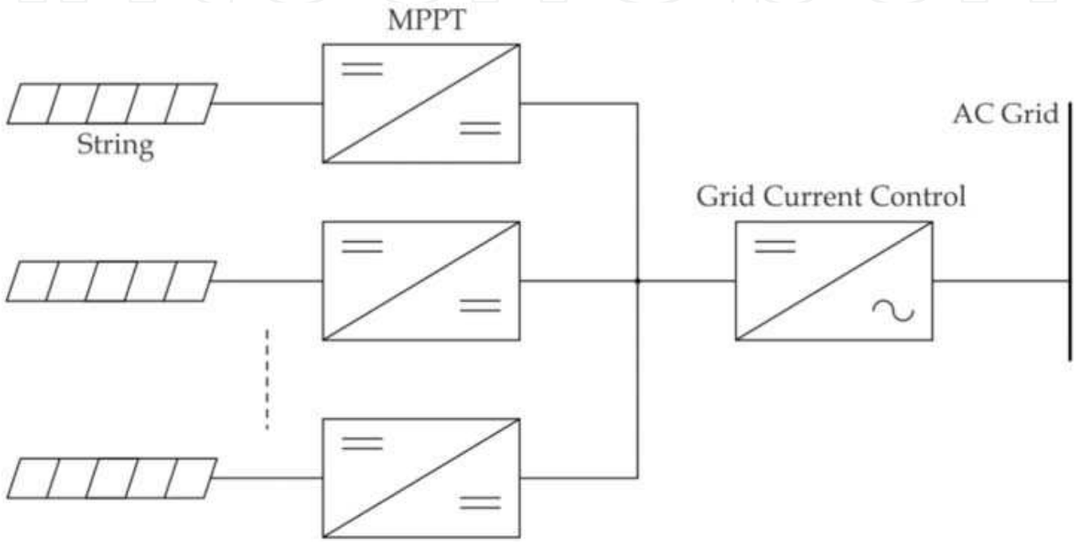

Fig. 3. Low power DC-DC converters connected to strings and one large DC-AC in the grid interface.

The inverters previously showed give an idea about the control and the DC-DC converters' application. It is worth discuss in more details how the PV modules are connected with inverters and these are connected with the grid. There are four configurations commercially accepted:

- Central-plant inverter: usually a large inverter is used to convert DC power output of PV array to AC power. In this system, the PV modules are serially string and several strings are connected in parallel to a single DC bus. A single or a dual-stage inverter can be employed. Fig. 4. illustrates this configuration.
- Multiple-string DC-DC converter: each string has a DC-DC converter, which can be galvanically isolated. There is a common DC link, which feeds a transformerless DC-AC converter. As Fig 5., only the multistage inverter can implement this configuration.
- Multiple-string inverter: several modules are connected in series on the DC side to form a string. The output from each string is converted to AC through a small individual inverter. Many such inverters are connected in parallel on the AC side. A single or a dual-stage inverter can be employed, as Fig. 6.
- Module-integrated inverter: each module has a small inverter. Once more, a single or a dual-stage inverter can be used. Fig. 7. shows this configuration.

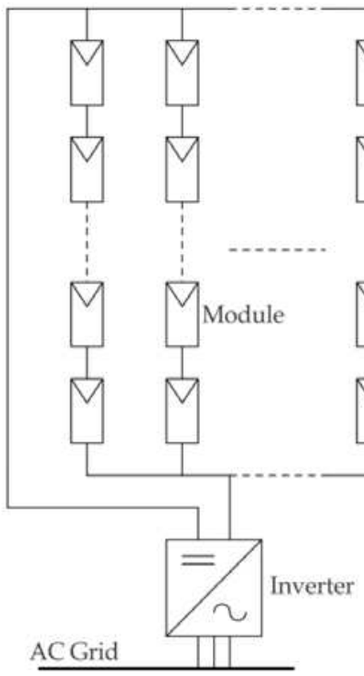

Fig. 4. Central-plant inverter.

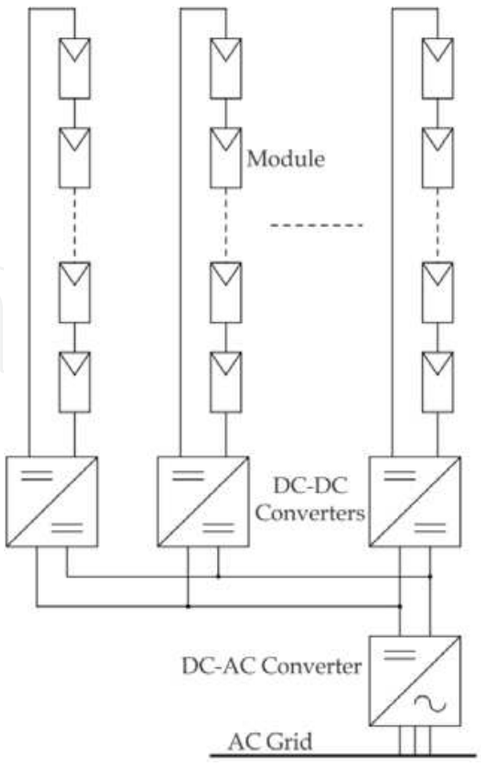

Fig. 5. Multiple-string DC-DC converter.

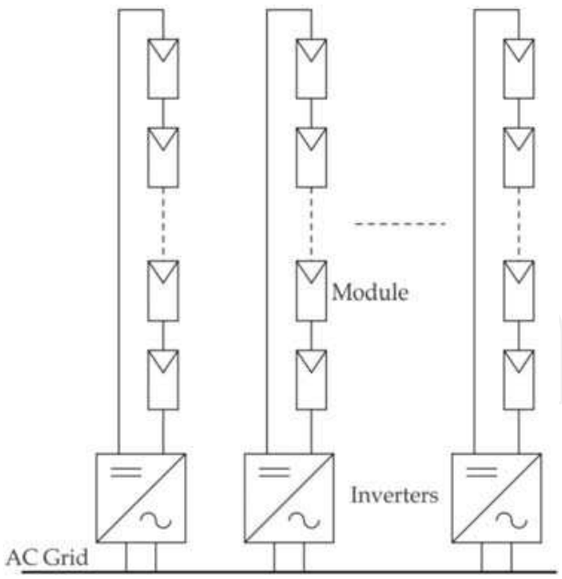

Fig. 6. Multiple-string inverter.

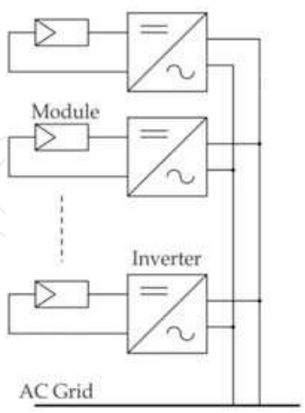

Fig. 7. Module-integrated inverter.

1.2 Considerations

The high efficiency is one of the most important characteristics of a PV inverter. Thus, whenever possible, these inverters are nonisolated electronic circuits, since a transformer

imposes an efficiency drop. This efficiency drop is 2% larger for a low than for a high-frequency transformer (Yuan & Zhang, 2005.). Hence, when grid-isolation is mandatory, the incorporation of a high-frequency transformer is a trend (Carrasco et al., 2006.).
As important as high efficiency, it is the inverter cost. Carrasco et al. (2006.) indicate the centralization of inverter for reduced cost, according to plant showed in Fig. 4.
To satisfies the previously argumentation, the dual-stage inverter configured in a central-plant is the solution. However, the MPPT will not be carried out by DC-DC stage. The system will be more cost-effective if it is able to track the MPP using the variables already available for the grid-current control. Some sensors would be avoided. Fig. 8. illustrates this simple idea. This implementation is discussed in the next section.

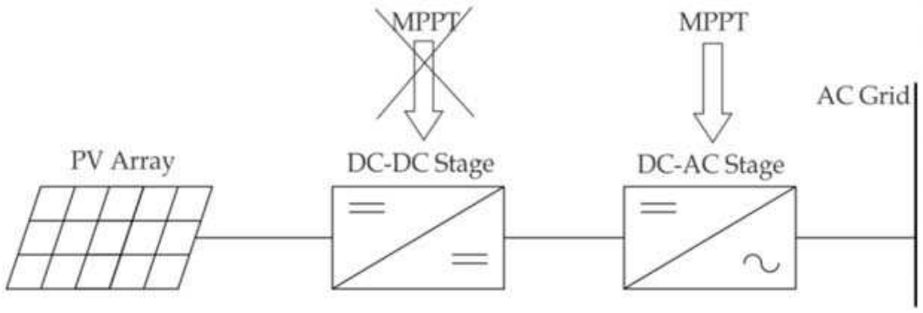

Fig. 8. Modified dual-stage inverter.

2. Behavior matching

The Behavior Matching Technique's purpose is to take a dual-stage inverter to perform the MPPT in the DC-AC stage, so that the control structure is simplified and the MPPT is improved. Normally, the DC-DC stage performs the MPPT in this type of PV inverter topology. From a didactic intent, the buck converter, showed in Fig. 9., is adopted to constitute the DC-DC stage. However, applying the Behavior Matching technique, all switch S parameters are constants. Therefore, duty cycle and switching frequency don't change during normal operation conditions.

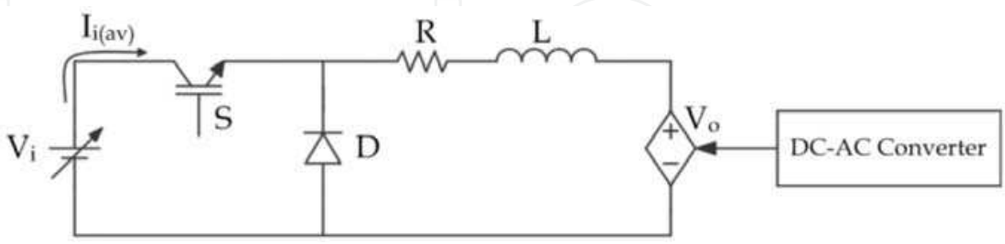

Fig. 9. DC-DC Buck converter.

The DC link voltage, V_o, is regulated by DC-AC stage. The feedback from V_o is compared with a reference defined by the MPPT algorithm. Hence, the controlled variable by the MPPT strategy is the DC link voltage.
It is well known that the ideal static gain of the Buck converter is given by $V_o' = D \cdot V_i$. Being V_o constant and V_i variable, the input average current, $I_{i(av)}$, goes to infinite when $D \cdot V_i > V_o$. For realistic input I-V characteristic, all Buck losses were represented by resistance R. Then,

this input I-V characteristic become inclined, as presented in Fig. 10. PV module's typical curves are in the background. For each irradiation level there is a MPP locus.
The DC-DC converter input I-V characteristic can fall together with MPP loci at various solar irradiation levels. Then, the convergence time of conventional MPPT algorithms is accelerated for rapid changes on insolation conditions. At the limit, no control action would be needed.
As noted in Fig. 10, a control action can shift the DC-DC converter input I-V characteristic for left or right, keeping its shape. Then, temperature variations of the PV module can be compensated with adjusts of the V_o value.

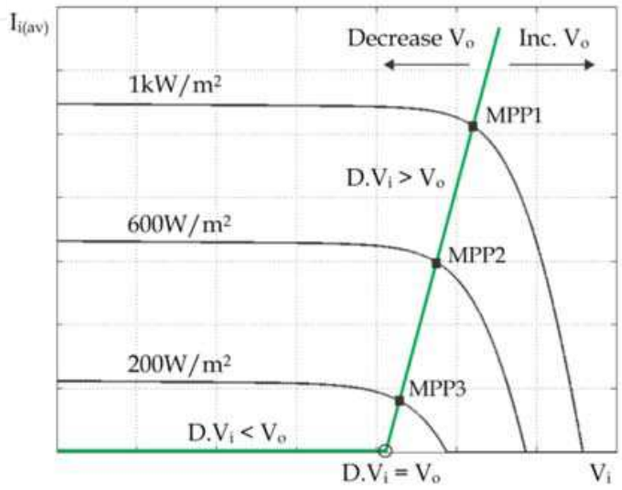

Fig. 10. DC-DC Buck converter input I-V characteristic on PV module curves.

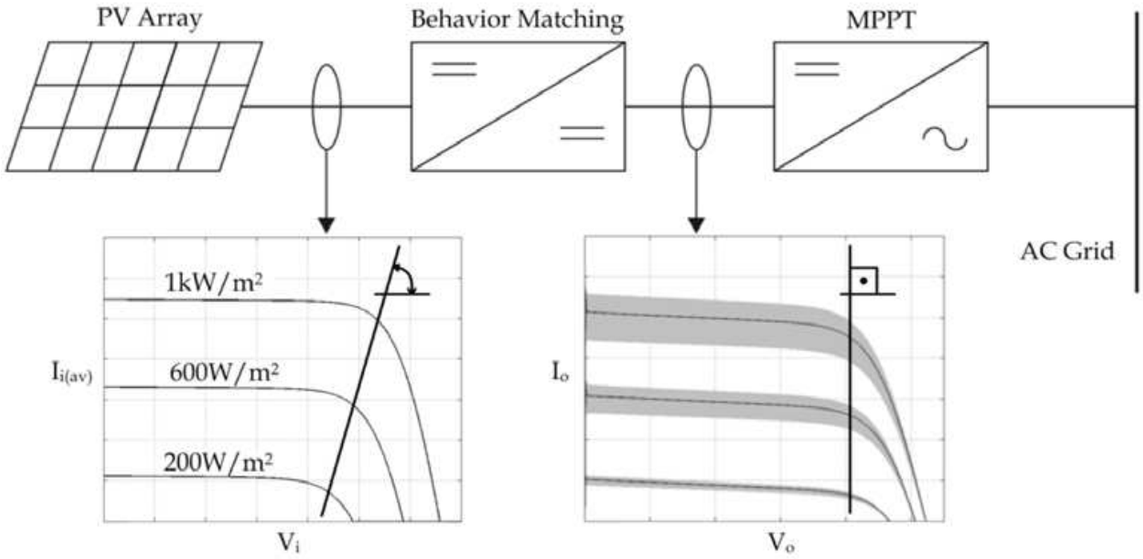

Fig. 11. Behavior Matching principles.

Fig. 11. shows simulation results where it can be seen that the PV array behavior, represented by $I_{i(av)}$ x V_i, is reproduced on the DC-DC stage output terminals, represented by

$I_{o(av)}$ x V_o. From the controller point of view, $I_{o(av)}$ x V_o is similar to $I_{i(av)}$ x V_i. Thus, MPPT task is to extract the maximum power of the DC link, or, to inject the maximum power in the grid. The strategies are different, but the result is the same: both tune the DC-DC stage input I-V characteristic to the PV array MPP.

The Behavior Matching Technique brings significant advantages for the PV system always that the DC-DC converter input characteristic curve lies on closest the MPP loci, for all MPPT range. Step-down DC-DC converters with similar input Buck behavior are eligible to integrate a modified dual-stage inverter.

3. DC-DC stage

The isolated ZVS Full-Bridge is usually used at power levels above 750W (Carrasco et al., 2006). Commonly, its efficiency ranges from 92% to 93% under a 45% to 100% load condition. With a nonisolated version, this efficiency can be increased within 96% to 98% (Lee et al., 2008). As an alternative to single-phase Full-Bridge based converters, the three-phase conversion has some advantages (Ziogas et al., 1988), such as:

- Reduced switching stresses of the power semiconductor devices.
- Reduced size and ratings of associated reactive components.
- Better transformer copper and core utilization.

The topic of this chapter focuses on the application of the three-phase isolated DC-DC series resonant converter (SRC3), proposed by Jacobs et al. (2004), in a dual-stage inverter. Despite the galvanic isolation, the measured efficiency of this DC-DC converter was above 97% under a 45% to 100% load condition.

The SRC3 topology is presented in Fig. 12. This three-phase DC-DC converter was evaluated about its efficiency in different input power levels, components number, EMI emission, performance under unbalanced conditions and power range. It seems to relate the best characteristics among others converters with soft commutation.

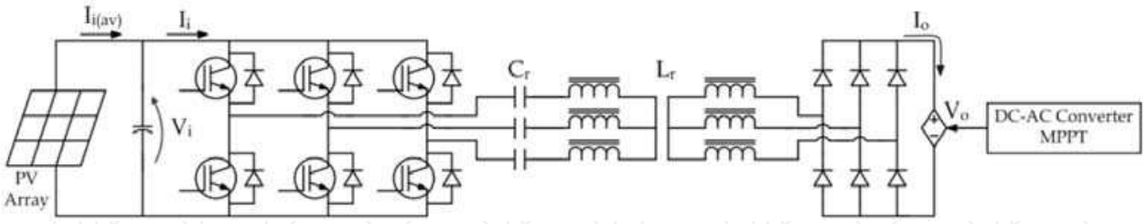

Fig. 12. Three-phase DC-DC Series Resonant Converter connected to a photovoltaic array.

The switches are gated by six phase-shifted signals. Neglecting the deadtime between two switches in each inverter leg, all switches are turned on exactly half a period.

When the switching frequency, f_1, is equal to the resonance frequency, f_r, the converter operates in ZCS mode. If $f_1 > f_r$, the converter operates in ZVS. In this condition, the efficiency is much reduced for low-power transfer. Then,

$$f_1 = f_r = \frac{1}{2 \cdot \pi \cdot \sqrt{L_r \cdot C_r}} \tag{1}$$

$$I_{i(av)} = \frac{6}{\pi^2 \cdot R_{loss}} \cdot \left(V_i - V_0^{'} \right) \tag{2}$$

Where:
L_r - leakage inductance of the transformer;
C_r - resonant capacitor;
V_o' – output voltage of the three-phase bridge rectifier, referred to the primary side;
R_{loss} - takes all losses into account: conduction and switching losses of the switches and diodes, the dielectric losses of the capacitors, the copper and iron losses of the three-phase transformer and the conduction losses of wires and connections.
The turns ratio transformer can be defined by : $N = N_2/N_1$.
The efficiency of the SRC3 strongly depends on the implemented deadtime and switching frequency. Beyond the designed values for them, the efficiency abruptly decreases. Consequently, these variables should not vary. Thanks the Behavior Matching, this is exactly the operation condition imposed to the converter.
The PV array consists of two parallel strings, each with ten KC200GT modules from Kyocera. Its nominal power is P_i = 4kW, with V_i = 263V and I_i = 15.2A. The estimated efficiency for the DC-DC stage is η_1 = 97%. The switching frequency of the SRC3 is f_1 = 40kHz. The grid has 220V of phase voltage.
The three-phase transformer is constructed with three single-phase transformers, in wye connection. The measured leakage inductances were L_r = 3.6μH. These result in resonant capacitors of C_r = 4.4μF, for ZCS operation. Polypropylene capacitors were adopted.
The nominal DC-link voltage is calculated with (3) and the converter losses with (4).

$$V_o' = \eta_1 \cdot V_i = 255V \tag{3}$$

$$R_{loss} = \frac{6}{\pi^2 \cdot I_{i(av)}} \cdot \left(V_i - V_o'\right) = 0.32\Omega \tag{4}$$

The voltage V_o' is raised to V_o = 816V by N = 3.2. This turns ratio keep the DC-link voltage above 600V for all MPPT range.
A SK20GD065 Semikron IGBT module was used. The diode bridge was made with six ultra fast recovery rectifiers FFPF05U120S, of 1200V and 5A.

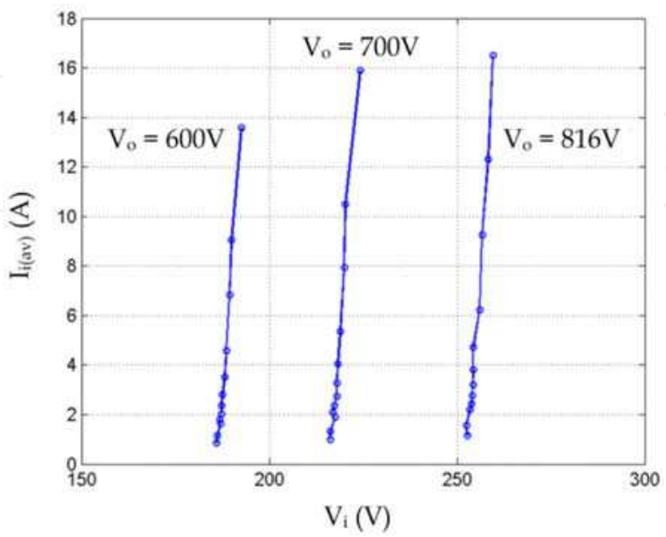

Fig. 13. DC-DC converter's input I-V characteristics.

The inclination of the SRC3 input I-V characteristic, for all Vo operation range, is given by (5), obtained from (2). Fig. 13. shows experimentally measured points of SRC3 prototype input I-V characteristic.

$$\frac{dI_{i(av)}}{dV_i} = \frac{6}{\pi^2 \cdot R_{loss}} = 1.9\frac{A}{V} \tag{5}$$

The DC-DC converter's input characteristic has a propitious behavior to MPPT algorithm. Putting Fig. 13. (V_o = 816V) on the PV array I-V characteristic curves, the proximity between the DC-DC converter's input characteristic and the MPP loci can be established, as shown in Fig. 14. This collaborates with the MPPT performance for fast changes in atmospheric conditions.

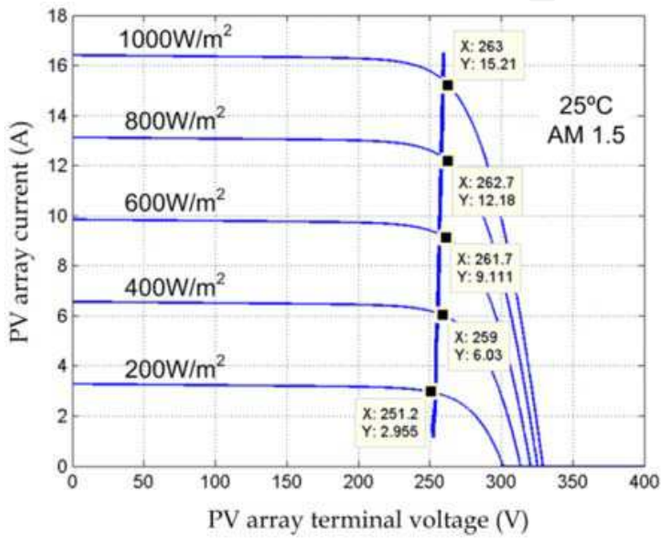

Fig. 14. Crossing between SRC3 and PV array characteristic curves.

4. Performance of the adopted DC-DC converter

A compare unit pertained to a peripheral of the Texas TMS320F2812 controller was configured to generate six gate pulses for SRC3, with duty cycle of 50% and deadtime of 640ns. The same DSP carried out the grid-current control and the MPPT.

Fig. 15. shows the resonant currents. Obviously, the leakage inductances of each phase are not exactly the same. These unsymmetries cause small differences in resonant currents amplitudes. However, this has a negligible impact on the SRC3 operation.

Figs. 16. and 17. present the DC-DC stage input and output currents for different power conditions. These currents have a low ripple and a frequency of six times that of the switching frequency, resulting in a continuous power flux. These features are not common among three-phase DC-DC converters and lead to reduced filter devices. The PV array parallel capacitor is of only 680nF, for example. The voltage ripple on it is showed in Fig. 18. This ripple was produced by the current I_i of Fig. 17. It has a negligible impact above PV array efficiency.

The ZCS commutation is shown in detail by Fig. 19. Unfortunately, the commutation losses drastically increase at low power levels, according to Fig. 20. Fig. 21. shows the SRC3 efficiency.

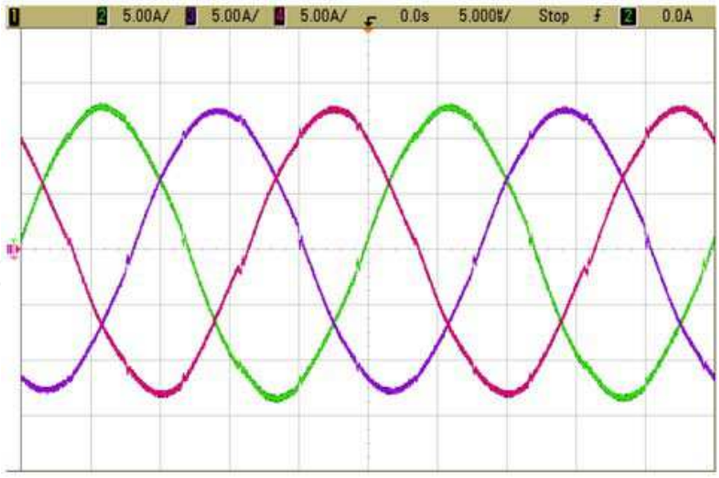

Fig. 15. Resonant currents under nominal conditions.

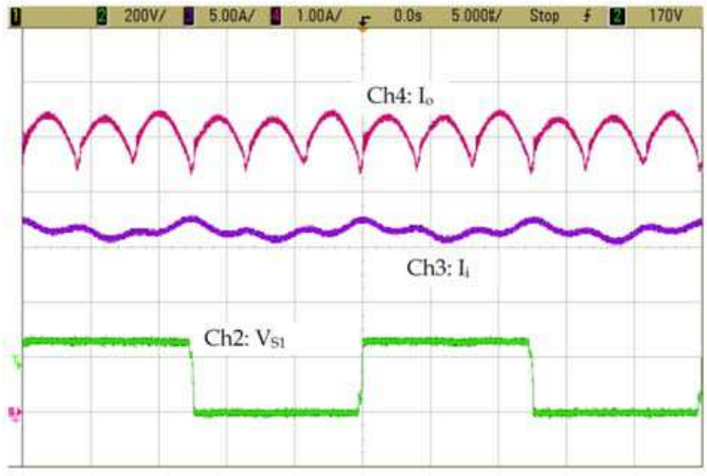

Fig. 16. DC-DC stage input and output currents and collector-emitter voltage, under nominal conditions.

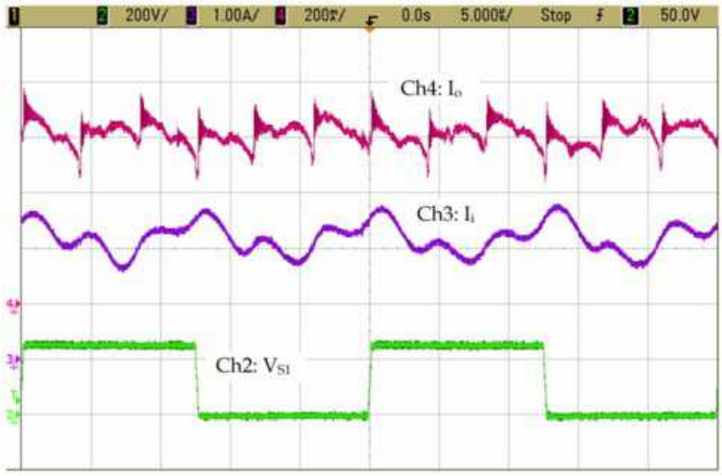

Fig. 17. DC-DC stage input and output currents and collector-emitter voltage, with P_o = 500W.

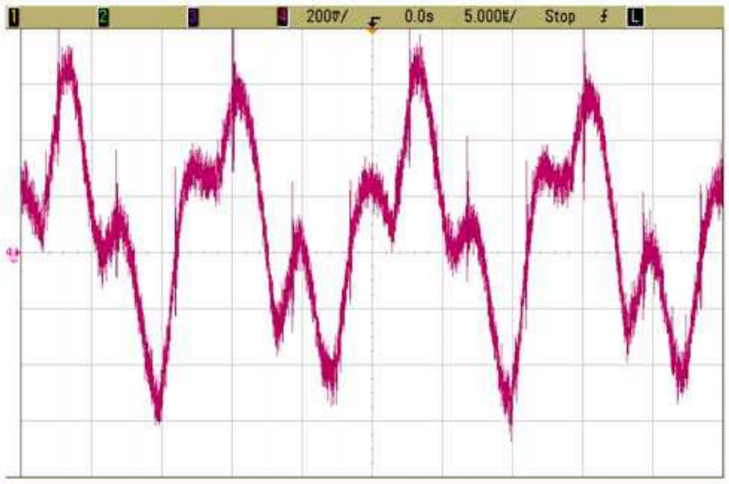

Fig. 18. PV array output voltage for P_o = 500W.

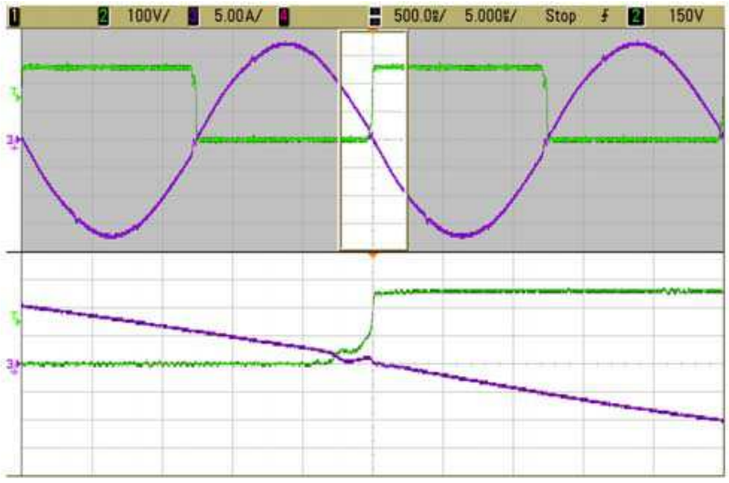

Fig. 19. Resonant current and collector-emitter voltage, under nominal conditions.

Fig. 20. Resonant current and collector-emitter voltage, for P_o = 500W.

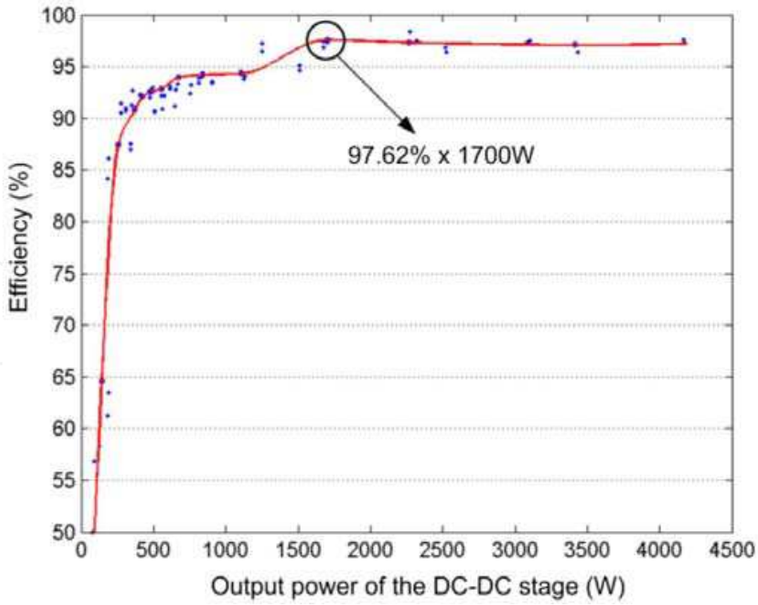

Fig. 21. SRC3 efficiency.

The impact of voltage harmonic components on the resonant current depends on the resonant circuit quality factor, presented in (6).

$$Q = 2 \cdot \pi \cdot f_r \cdot \frac{L_r}{R_{loss}} \tag{6}$$

The requirement of large impedance for frequencies that are different of the resonant frequency is fulfilled when the quality factor Q is high. The value of Q is high in nominal conditions, such as Fig. 19. On the other hand, for low SRC3 output power rate, the Q value is low too, according to Fig. 20. This occurs due increasing of R_{loss} for output powers below of approximately 1700W. Fig. 21 points to decreasing of efficiency below this power. Larger L_r could reduce the power from which R_{loss} rises. The efficiency would be more flat.

5. Conclusion

This chapter proposed the Behavior Matching technique applied to grid-connected photovoltaic systems composed of dual-stage inverters. A dual-stage inverter contains DC-DC stage and DC-AC stage. Through the Behavior Matching, the DC-DC stage operates with constant frequency and duty cycle and the DC-AC stage becomes responsible for the maximum power point tracking and grid-current control. The I-V characteristic of PV array was reproduced at output of the DC-DC stage, without any control. Some sensors could be avoided because the grid-current control apparatus produces the variables needed for the MPPT. In addition, only one digital controller can generate gate pulses for all transistors of PV system, which results more simple and cheaper. It was demonstrated if a propitious converter composes the DC-DC stage, the MPPT convergence remains faster for rapid changes in solar irradiation power. Among various soft switching three-phase DC-DC converters, the Series Resonant was selected for practical analysis. It added a lot of advantages for PV system. Its efficiency is highest for a specific frequency and its duty cycle

cannot change. Thus, Behavior Matching optimized it along all operation range. This input I-V characteristic matched with MPP loci, without any control action. The converter can switch with high frequencies, 100kHz or more, becoming very compact, i.e., its transformer and capacitors. An insignificant capacitor was used on implementation of PV array parallel filter. Two factors mainly contributed with this advantage: the continuous current flux with low ripple and the barrier formed by the resonant circuit to electrical perturbations on DC link, that did not affect the primary side voltage bus. Finally, the Series Resonant Converter features a robust operation under unbalanced conditions.

6. References

Casaro, M.M. & Martins, D.C. (2007). New Method of MPPT Application for Dual-Stage Inverters, *9th Brazilian Power Electronics Conference*, pp. 676-681.

Casaro, M.M. & Martins, D.C. (2008). Behavior Matching Technique Applied to a Three-Phase Grid-Connected PV System, IEEE International Conference on Sustainable Energy Technologies, pp. 17-22.

Carrasco, J.M.; Franquelo, L.G.; Bialasiewicz, J.T.; Galván, E.; Guisado, R.C.P.; Prats, M.A.M.; León, J.I. & Moreno-Alfonso, N. (2006). Power-Electronic Systems for the Grid Integration of Renewable Energy Sources: A Survey. *IEEE Transactions on Industrial Electronics*, Vol. 53, No. 4, August 2006, pp. 1002-1016.

Jacobs, J.; Averberg, A. & De Donker, R. (2004). A Novel Three-Phase DC/DC Converter for High-Power Applications, *IEEE Power Electronics Specialists Conference*, pp. 1861-1867.

Lee, J.; Min, B.; Kim, T.; Yoo, D. & Yoo, J. (2008). A Novel Topology for Photovoltaic DC/DC Full-Bridge Converter with Flat Efficiency Under Wide PV Module Voltage and Load Range. *IEEE Transactions on Industrial Electronics*, Vol. 55, No. 7, July 2008, pp. 2655-2663.

Yuan, X. & Zhang, Y. (2005). Status and Opportunities of Photovoltaic Inverters in Grid-Tied and Micro-Grid Systems, *15h International Photovoltaic Science & Engineering Conference*, pp. 226-227.

Ziogas, P.D.; Prasad, A.R. & Manias, S. (1988). Analysis and Design of a Three-Phase Off-Line DC/DC Converter with High Frequency Isolation, *Proceedings of IEEE Industry Applications Society*, pp. 813–820.

Paths to Sustainable Energy
Edited by Dr Artie Ng

ISBN 978-953-307-401-6
Hard cover, 664 pages
Publisher InTech
Published online 30, November, 2010
Published in print edition November, 2010

The world's reliance on existing sources of energy and their associated detrimental impacts on the environment- whether related to poor air or water quality or scarcity, impacts on sensitive ecosystems and forests and land use - have been well documented and articulated over the last three decades. What is needed by the world is a set of credible energy solutions that would lead us to a balance between economic growth and a sustainable environment. This book provides an open platform to establish and share knowledge developed by scholars, scientists and engineers from all over the world about various viable paths to a future of sustainable energy. It has collected a number of intellectually stimulating articles that address issues ranging from public policy formulation to technological innovations for enhancing the development of sustainable energy systems. It will appeal to stakeholders seeking guidance to pursue the paths to sustainable energy.

INTECH
open science | open minds

InTech Europe
University Campus STeP Ri
Slavka Krautzeka 83/A
51000 Rijeka, Croatia
Phone: +385 (51) 770 447
Fax: +385 (51) 686 166
www.intechopen.com

InTech China
Unit 405, Office Block, Hotel Equatorial Shanghai
No.65, Yan An Road (West), Shanghai, 200040, China
中国上海市延安西路65号上海国际贵都大饭店办公楼405单元
Phone: +86-21-62489820
Fax: +86-21-62489821

IntechOpen